2018
International Symposium on Power Electronics,
Electrical Drives, Automation and Motion

Identification of Linear Permanent Magnet Synchronous Motor Parameters and Inverter Non-Linearity Effects

Shafiq Odhano, Mi Tang, Andrea Formentini, Pericle Zanchetta
Department of Electrical and Electronic Engineering
The University of Nottingham
Nottingham, United Kingdom

Radu Bojoi
Department of Energy
Politecnico di Torino
Turin, Italy

***Abstract*—The paper presents an automatic parameter identification procedure for linear permanent magnet synchronous motors. The electrical parameters of a test machine are estimated by identification tests performed through the inverter. The method employs the available feedback signals that are needed by the control. The stator resistance and machine inductances are estimated through signal injection at standstill. The permanent magnets' flux-linkage identification instead requires carriage movement. Subsequently, the inverter non-linearity characteristics are identified, again at standstill, through a flux-observer. The proposed self-commissioning process requires only the nameplate data of the machine and no datasheet information of the power electronic devices is needed. The developed techniques can be used both with and without a position sensor. The complete process is automatic and safe to run on its own and requires least intervention from the operator.**

Keywords—inverter non-linearity, linear machines, parameter estimation, permanent magnet machines, servomotors, variable speed drives

I. INTRODUCTION

Rotary permanent magnet synchronous machines (PMSMs) are commonly used in actuators and servomechanisms due to their fast dynamic response and the ability to work at zero speed for prolonged periods without overheating. Even in applications that demand continuous rotation, their use is steadily increasing for their higher efficiency and better power factor, compared to a rotary induction machine for instance. The aforementioned advantages offered by permanent magnet (PM) excitation are equally adaptable for linear machines. In fact, in servo-applications, the superior dynamic performance of PMSMs is of even greater value in linear actuation than it is in case of rotary mechanisms. The foremost reason for this lies in the construction and operation of the machine itself in that it does not move *infinitely* in one direction if the track length is limited. At the end of the track, the carriage has to reverse the direction or pass on to a new set of stator windings or magnet sections (depending on the machine construction). With permanent magnets mounted on the mobile part of the motor, which is usually the case with 'longer' machines, the control has to switch to the adjacent set of windings to continue propulsion beyond the reach of previous set of windings. In designs where the mobile part carries windings, the control does not have to switch windings; however, the cost of such designs gets unreasonably high due to the price of permanent magnet material if long track lengths are needed. Nevertheless, for industrial automation where the reach of a single permanent magnet linear synchronous motor (PMLSM) is limited, under 10 metres [1], the latter design (with mobile armature) is a preferred choice to simplify the control.

Whether it is a rotary PMSM or a linear actuator, the parameters' information plays a decisive role in the performance of control. Where high-performance control is needed, it is inevitable to have accurate values of machine's electrical and mechanical parameters. Whereas the mechanical parameters (not discussed in this paper) such as inertia and friction constants decide the quality of position and speed control, the performance of current control is governed by the electrical and magnetic parameters of the machine. These include stator resistance, machine inductance as a function of position and the permanent magnet flux-linkage. Furthermore, like the rotary machines, linear PMSMs are, in most cases, driven by power electronic converters. The converter's switches, being non-ideal semiconductor devices, have voltage drop across them that is a function of current. The voltage error introduced by power devices, if not compensated appropriately, can have deleterious effects on current control performance. All these factors highlight the importance of identifying the system parameters before being able to design appropriate controllers.

Parameter identification of PMLSMs through the inverter is not widely covered in the literature, nevertheless, there are a number of identification methods that are available for rotary PMSMs that can be adopted for these machines. However, it must be noted that only those parameter estimation techniques of rotary machines can be considered for PMLSMs that do not require continuous shaft rotation. Estimation methods identifying parameters at standstill can be a preferred choice such as those used in [2] and [3] for inductance and resistance estimation. In [2], for stator resistance estimation, a constant voltage at two different magnitudes is applied along the *d*-axis and the resulting current is measured. The resistance is obtained through the ratio of voltage and current differences. Similarly, *d*- and *q*-axis inductances are obtained through the

S. Odhano, M. Tang, A. Formentini and P. Zanchetta would like to acknowledge the support of Best Motion Technology, Shenzhen, China, for this research.

978-1-5386-4941-1/18/$31.00 ©2018 IEEE

application of short voltage pulses along the *d*- and *q*-axis, respectively. The rate of change of current is captured during the voltage pulse injection and the inductance of each axis is calculated from the ratio of the applied voltage and the current derivative. This test is also performed at two different voltage levels to cancel out the inverter switches' voltage drop effect. However, the use of open-loop voltage pulses may cause current protection trip in case of low-reactance machines. For the PM flux identification, a constant *q*-axis current is applied and the controller output voltage is used to get the back-emf constant of the machine that is proportional to the PM flux-linkage value.

Flux-linkage self-identification methods of [4, 5] proposed for synchronous reluctance and interior permanent magnet machines can also be used for *d*- and *q*-axis inductances' identification at standstill for linear PM machines. The method presented in [4] requires the application of a square wave current waveform, along *d*- and *q*-axis, through proportional-integral (PI) controllers and the recording of the controller output voltage. The flux-linkage along each axis is obtained through the offset-free integration of controller output voltage after eliminating stator resistance drop and inverter non-linearity errors. The identification scheme of [5] proposes square wave voltage pulses injection for the computation of flux-linkage curves of the machines. The flux-linkage is obtained through integration, as in [4]. However, an analytical approximation function is defined for relating the flux-linkage to current and the parameters of this function are obtained through offline post-processing of the acquired data. As said above for [2], the open-loop voltage injection requires careful consideration when dealing with low-reactance machines.

Standstill self-commissioning strategies of [6] that use sinusoidal current injection to get inductance of each orthogonal axis of the machine, can be adopted for PMLSM under consideration, however, the post-processing of the acquired data might be a limiting condition when the self-commissioning routines are to be embedded in the control algorithm. The differential inductance estimation part of the magnetic model identification technique of [7], proposed for rotary surface mounted and interior permanent magnet synchronous machines, can be harnessed for the self-identification of inductances also in linear PM machines. However, the dc-bias along *q*-axis needs to be dealt with care as the unloaded linear motor carriage might not have enough mass to filter out the force pulsations produced by the square-wave current proposed in [7].

Other identification techniques for machine inductances and PM flux-linkage are reviewed in [8] and [9]. However, none of the methods surveyed above present a complete self-commissioning solution including the identification of the inverter model. For inverter non-linearity identification, there are dedicated identification techniques found in the literature. For instance, [10] presents self-commissioning of inverter dead-time effects with a physical model, the physical model being the connected machine. In [11], the authors have presented a self-tuning algorithm for inverter model coefficients for accurate compensation. Similarly, in [12-15] inverter error identification is performed for enhancing the sensorless control of rotary machines.

This paper presents a complete self-commissioning routine for machine's electrical parameters as well as the inverter non-linearity effects for a linear permanent magnet synchronous machine having a limited track length. The proposed method uses a controlled current strategy for all parameter estimation steps. The stator resistance is identified the same way as in [2] but with current control that renders the method suitable for high-power low-resistance machines. The *d*- and *q*-axis inductances are estimated through sinusoidal current injection using resonant controllers. The standstill condition during *q*-axis inductance estimation is ensured by injecting a sufficiently high frequency (e.g. 500Hz) to avoid sustained rotor movement.

The PM flux-linkages' identification needs carriage movement to get induced emf in the stator windings that can be used to compute the flux. For this test, a current vector is set up along *d*-axis which is then rotated at a controlled constant frequency for the mover to follow. The current in the *q*-axis is controlled to zero and the controller output voltage is acquired, from which the PM flux-linkage is estimated. Finally, for the inverter non-linearities self-commissioning, a PM flux observer is proposed, which is used to minimize the error between the observed and known PM flux. The correction term introduced by the observer gives the error caused by the inverter non-linearity effects.

The proposed method automatically identifies parameters with tests conducted through the inverter and does not require any post-processing. The identification tests are performed on two PMLSMs with moving armature and stationary excitation (PMs).

II. PMLSM And Inverter Model

Similar to a rotary motor, the simplest equivalent circuit of a PMLSM can be represented in rotor/mover *dq*-axes as shown in Fig. 1. The convention of normal PM machines is used in which the *d*-axis is aligned with the north pole of permanent magnets. The core losses' branch is neglected for simplicity. The voltage equations in the *d*- and *q*-axis are:

$$u_d = R_s i_d + L_d \frac{di_d}{dt} - 2\pi \frac{v}{\tau} L_q i_q \tag{1}$$

$$u_q = R_s i_q + L_q \frac{di_q}{dt} + 2\pi \frac{v}{\tau} \left(L_d i_d + \lambda_m \right) \tag{2}$$

where R_s is stator resistance, u, i, and L are voltage, current, and inductance, respectively, with subscripts d and q indicating the axis while λ_m is the permanent magnet flux-linkages in Vs. The linear speed v is measured in m/s and τ is twice the pole-pitch (i.e. the distance between two consecutive north poles, in metres, on the (stationary) permanent magnet strip).

The voltage error introduced by the inverter is divided mainly in two components: the error due to dead-time and the error caused by the voltage drop in the on-state resistance of the power devices. The literature treats in detail the modelling and analysis of these errors, so they are not presented in detail

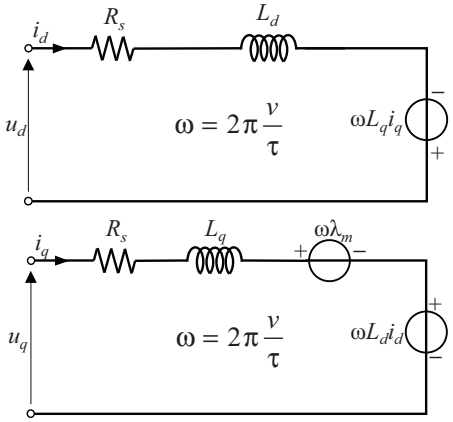

Fig. 1. PMLSM equivalent circuit: *d*-axis (top), *q*-axis (bottom).

here. The voltage error Δu, in phase quantities, introduced by inverter switches can be represented as follows:

$$\Delta u = U_{th}\left(\mathrm{sgn}(i)\right) + R_{on} i \tag{3}$$

where U_{th} is the device threshold voltage that depends on the sign of the phase current i and R_{on} is the on-state resistance of the power electronic switch. There are different ways in which equation (3) is used for inverter error compensation. Some researchers model it as an approximate exponential function, others use tangent-hyperbolic function approximation, yet others record the voltage error at different current values and construct a look-up table. This paper follows the look-up table approach. However, the way in which this look-up table is identified is different from available identification schemes.

III. Machine Parameter Identification

To devise efficient control strategies from voltage equations (1) and (2), it is necessary to have correct machine parameters, namely, R_s, L_d, L_q, and λ_m. The test procedure for the identification of these parameters is now presented.

A. Stator resistance estimation

A simple and reliable method of estimating stator resistance, R_s, is to use a dc injection test at two different current levels, or voltage levels as in [2], of the same sign. The resistance is obtained from the ratio of voltage and current differences. However, the open-loop voltage application of [2] leaves the current as an uncontrolled quantity that could result in excessive current for low impedance machines. A closed-loop current control is preferable as it allows limiting the current to below protection threshold. The controller can be tuned roughly (based on inductance estimate from nameplate data) for this test as the control dynamics are not critical and only steady state values of voltage and current are needed for resistance estimation. To prevent carriage movement during this test, the current is injected along the *d*-axis.

By performing the test at two current levels, without changing the sign of the current, the inverter voltage error can be excluded, at least the U_{th} part in (3). However, it is not possible to separate R_s from R_{on}, but, since the overall system always consists of $R_s + R_{on}$, this does not pose significant problems for control design. Furthermore, R_{on} is usually very small compared to typical machine resistances: for instance, in the studied case, R_{on} is about 20mΩ and the machines' resistances are around 2Ω. So, R_{on} can be lumped together with R_s for practical reasons.

B. Inductances' identification

The *d*- and *q*-axis inductances' identification is performed through the injection of sinusoidal current signals along respective axes. A proportional-resonant controller is used to achieve this. The total impedance along each axis is calculated through the voltage reference and the measured current. To separate inductive reactance from the total impedance, the phase angle between voltage and current is needed for which data post-processing might be necessary [6]. However, if the reactive power equation (4) is used, the need for post-processing can be completely eliminated. Thus, the inductive reactance, and hence inductance, can be computed in real time using (5).

$$Q = u_y i_x - u_x i_y \tag{4}$$

$$L_{d/q} = \frac{Q}{\omega_{res} i_{d/q}^2} \tag{5}$$

In (4), the subscripts *x*, *y* denote the two orthogonal components of voltage and current vectors. The *xy* components of voltage are obtained directly from the integrator states of the proportional-resonant controller as shown in Fig. 2 while those of current are taken through a resonant filter as in Fig. 3. In (5) and in Fig. 2 and 3, ω_{res} is the resonant frequency which is the same as current injection frequency for inductance estimation. In Fig. 2, k_p and k_{res} are proportional and resonant controller gains, respectively. The use of resonant filter for obtaining the orthogonal component of a sinusoidal quantity is well known in the literature. It is most commonly used for single phase grid-connected applications. Structurally, the resonant filter of Fig. 3 is identical to a second order generalized integrator of [16] and [17].

Inductance identification tests through sinusoidal current injection along the *d*-axis does not produce any force that displaces the carriage. However, along the *q*-axis a non-zero instantaneous force will be generated that would result in oscillatory carriage movement, even though the net displacement can still be zero if a zero-mean current signal is injected. To ensure that the carriage is unmoved, the frequency of the injected signals needs to be sufficiently high for the generated force to be filtered out by carriage mass.

It can be noticed from the above discussion and Fig. 2 that the voltage command given by proportional-resonant controller is directly used for inductance estimation even if the inverter non-linearity effects have not been identified and compensated yet. This does not cause any error in the inductance calculation since the inverter error affects only the real part [18] of the impedance. Thus the method described above using the reactive power is immune to inverter non-linearity errors.

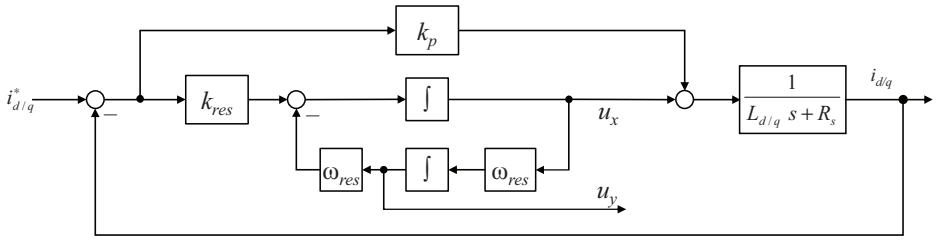

Fig. 2. Proportional-resonant controller for current control.

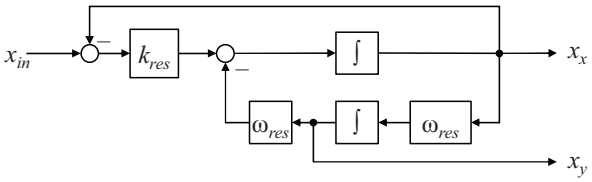

Fig. 3. Resonant filter to get current *xy* components.

C. PM flux-linkage estimation

For this test, the movement of the carriage is necessary. However, this movement can be controlled and the test can be carried out even if there is a load on the machine equal to the rated force. Starting from one end of the track, a *d*-axis current close to the rated machine current is applied, while the *q*-axis current reference is held equal to zero. The current vector, aligned with the north pole of the magnets, is moved at a controlled constant speed towards the other end of the track. During this movement, the carriage follows the current vector. To regulate the *q*-axis current to zero, the current controller outputs a voltage that is required to counter the induced back-emf due to PMs and the cross-coupling term of the *d*-axis current (2). Knowing the linear speed of the mover and the applied *d*-axis current as well as the *d*-axis inductance estimated in the previous step, the PM flux can be obtained by rearranging (2) using (6).

$$\lambda_m = \frac{\tau}{2\pi v} u_q - L_d i_d \tag{6}$$

It must be noted that as the current in the *q*-axis is controlled to zero, ideally there is no effect of stator resistance as well as the inverter non-linearity effects on the results. But practically, as the *q*-axis component of the uncompensated inverter non-linearity effects is a saw-tooth wave [19], the voltage given by the *q*-axis controller will have a saw-tooth wave-shape as well with the back-emf dependent component superimposed. The PM flux-linkage can still be estimated by taking the mean value of this voltage over a distance equal to τ (i.e. twice the motor pole-pitch).

IV. Inverter Non-Linearity Self-Commissioning

Having identified the parameters of the connected machine, the load-side model can be assumed *completely defined*. Now, the inverter non-linearity effects can be identified through a standstill test. The mathematical bases for the identification process is formulated starting from the flux-linkage in the synchronous *dq*-reference frame whose *d*-axis is aligned with

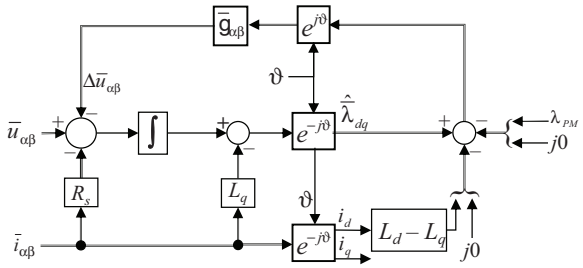

Fig. 4. PM-flux observer scheme for identifying inverter non-linearity effects.

the north pole of the magnets:

$$\lambda_d + j\lambda_q = L_d\ i_d + \lambda_m + jL_q\ i_q$$

transforming it to αβ frame

$$\bar{\lambda}_{\alpha\beta} = e^{j\vartheta}\left(L_d\ i_d + \lambda_m + L_q\ i_d - L_q\ i_d + jL_q\ i_q\right)$$

rearranging and simplifying:

$$\lambda_m + j0 = e^{-j\vartheta}\left(\bar{\lambda}_{\alpha\beta} - L_q\ \bar{i}_{\alpha\beta}\right) - \left(L_d - L_q\right) i_d \tag{7}.$$

Eq. (7) is used as a PM flux-linkage observer and is the basis of inverter identification tests. The identification scheme can be designed as shown in Fig. 4 where the flux-linkage given by (7) is compared with the known PM flux identified in the previous step. The difference is passed through a gain vector $\mathbf{g}_{\alpha\beta}$ which corrects the error. With all other parameters defined, this error can be attributed to the inverter non-linearity effects. Performing tests at various current levels leads to the identification of $\Delta u_{\alpha\beta}$ as a function of current.

TABLE I. Test Machines' Data

Machines data		
Quantity (unit)	***PMLSM 1***	***PMLSM 2***
Rated force (N)	80	125
Rated current (A_{pk})	3.65	3.7
Stator resistance (Ω)	1.9	2.4
d-axis inductance (H)	0.0073	0.0106
q-axis inductance (H)	0.0079	0.0101
PM flux-linkage (Vs)	0.076	0.111

V. Experimentl Results

The machines used for experiments are two linear motors of different dimensions, whose detailed data is given in Table I. One machine is used without any load while the other has load mass attached to it. The mover position in each case is available through an incremental encoder with a resolution of 0.5 µm. The control algorithm is executed on a custom-built control platform [20]. The power converter is a commercial 2 kW drive from Best Motion Technologies, appropriately modified to allow external control of power electronic switches through fiber optic signals. The complete experimental setup is not shown here due to space constraints.

A. Identification of stator resistance

Fig. 5 shows the measured current and controller voltage command along mover *d*-axis for resistance estimation of PMLSM 2. To eliminate measurement noise, the measured current and controller voltage are averaged over a period of time after steady state is reached. The resistance is estimated from the ratio of voltage and current differences of Fig. 5 and for motor 2, it is found to be 2.45 Ω having an error of less than 3% when compared to the data given in Table I.

B. dq-axes inductances' estimation

The inductances of PMLSM 1 are identified as per the method described in section III above. The test current amplitude is fixed but can be varied to estimate inductance as a function of current for saturation effects. Fig. 6 gives the test results for a 500 Hz test frequency and 1 A current amplitude injected along the *d*-axis. The middle axis shows the resonant filter states given by Fig. 3 when the input is the measured *d*-axis current. The bottom axis gives the *d*-axis voltage output by the proportional-resonant controller of Fig. 2 as well as its orthogonal component. It can be observed that after initial transient the current and voltage orthogonal components are in steady state and (4) can be applied to get the reactive power from which L_d is obtained using (5). Fig. 7 gives the computed reactive power (top) and the estimated *d*-axis inductance (bottom). It can be readily observed that the estimated inductance is about 7.4 mH which closely corresponds to the known value from Table I. It must be noted that the horizontal scale in Fig. 7 is different from that of Fig. 6. In Fig. 6, the scale is zoomed in to show less cycles for visual clarity.

For the *q*-axis inductance identification, the results are presented in Fig. 8. For brevity, the current and voltage waveforms similar to Fig. 6 are excluded and only the reactive power (top) and L_q (bottom) are shown. In Fig. 8, it can be observed that the *q*-axis inductance is about 8 mH i.e. an error of about 1% with respect to the value given in Table I.

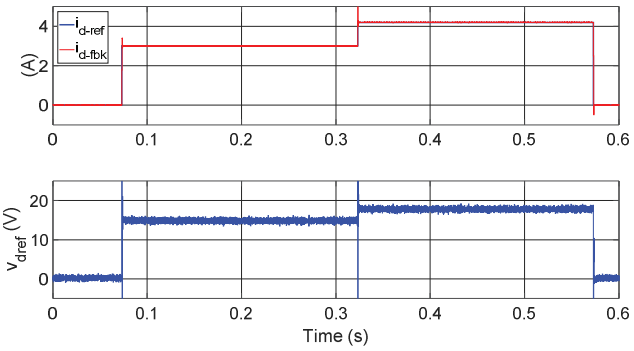

Fig. 5. PMLSM 2 stator resistance estimation – top: reference and feedback *d*-axis current, bottom: controller output votlage.

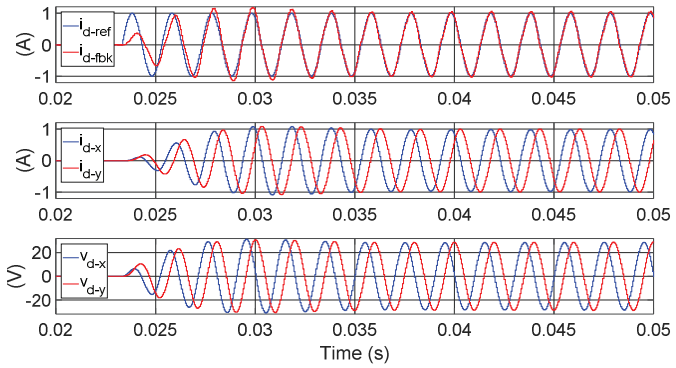

Fig. 6. PMLSM 1 *d*-axis inductance identification – top: reference and feedback *d*-axis current, middle: orthogonal components of *d*-axis current, bottom: controller output voltage and its orthogonal component.

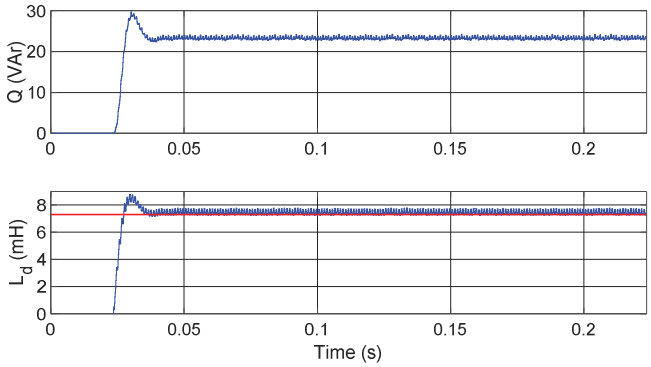

Fig. 7. PMLSM 1 *d*-axis inductance identification – top: reactive power given by (4), bottom: *d*-axis inductance obtained using (5), the red line shows the known value.

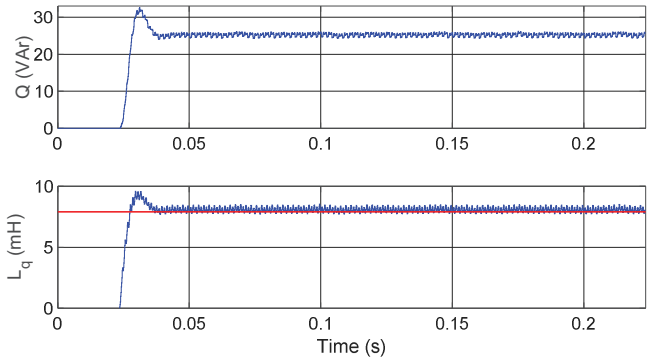

Fig. 8. PMLSM 1 *q*-axis inductance identification – top: reactive power given by (4), bottom: *q*-axis inductance obtained using (5), the red line indicates the known value.

As noted from the lower plots of Fig. 7 and 8 the inductance value is readily available in real time unlike requiring the post-processing of [4–7]. This helps embed the inductance identification algorithm in the start-up routine without requiring any data acquisition and post-processing on part of the user. Besides, the estimated inductance value reaches steady state within 10 periods of injection frequency.

Any spurious noise on the estimates can be removed by averaging over a few cycles after steady state is reached. Besides, the results of Fig. 7 and 8 confirm that the inverter non-linearity effects, even if left uncompensated, do not influence the reactive power and therefore the estimation of inductances.

C. PM flux estimation

The method described in section III-C is used for the estimation of PM flux-linkage. Fig 9 (top) shows the constant *d*-axis current which is established to align the mover with the north pole of PM strip and the *q*-axis current that is held at zero. Afterwards, the current vector is moved in a controlled way, as shown by the phase currents in the lower plot. The *q*-axis voltage and the linear speed are shown in Fig. 10. As observed, the speed is not constant due to the fact that the speed is not closed-loop controlled but an open loop control is used. These speed oscillations may be due to the cogging force. The *q*-axis voltage, shown in the lower plot, has the typical saw-tooth shape due to inverter non-linearity effects (six periods in one electrical cycle). Nevertheless, the constant part of the voltage on which the saw-tooth wave is superimposed can be easily identified. Note that the horizontal scale in Fig. 10 is zoomed in with respect to Fig. 9 to show *q*-axis voltage clearly. The PM flux-linkage value obtained from the data (after averaging) of Fig. 9 and 10 using (6) is found to be 0.116 Vs, which gives an error of less than 5% when compared with the known flux value.

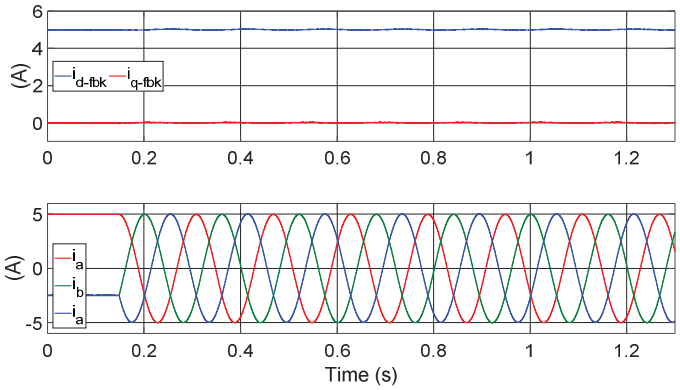

Fig. 9. PMLSM 2 PM flux-linkage identification procedure – top: measured *d*- and *q*-axis currents, bottom: phase currents.

D. Inverter non-linearity characteristic identification

The voltage error introduced by inverter dead-time and device voltage drops can now be identified using the method described in section IV as all the unknown parameters of Fig. 4 have been identified. The method can be used either by injecting a sinusoidal current of varying amplitude or a current ramp. The results presented here use a current ramp. Fig. 11 shows the test results at the nominal dc-link voltage (300 V) with the switching frequency of 10 kHz and the inverter dead-time equal to 2.5 µs. The test is conducted through phases B and C that leaves the current through phase A equal to zero. Consequently, the inverter error voltage appears only in the β-axis as shown in the lower plot of Fig. 11.

The test is repeated for a switching frequency of 16 kHz

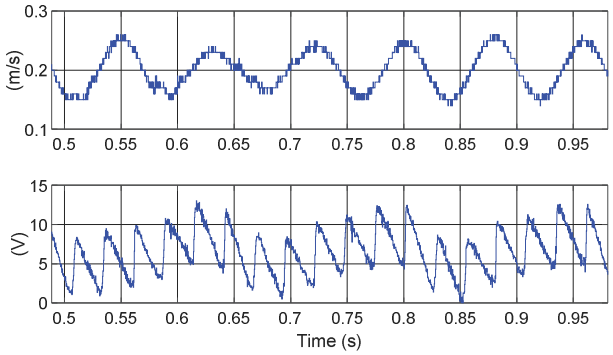

Fig. 10. PMLSM 2 PM flux-linkage identification – top: linear speed, bottom: *q*-axis reference voltage.

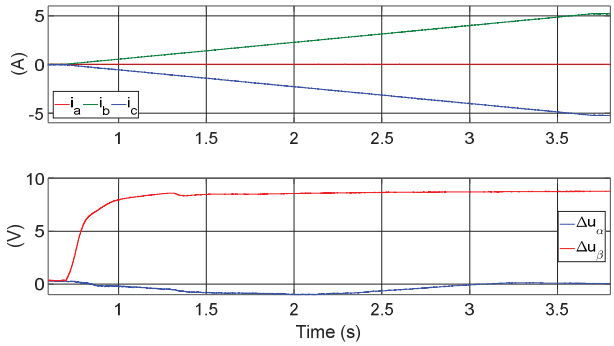

Fig. 11. Inverter non-linearity characteristic identification – top: phase currents, bottom: α and β components of the error voltage.

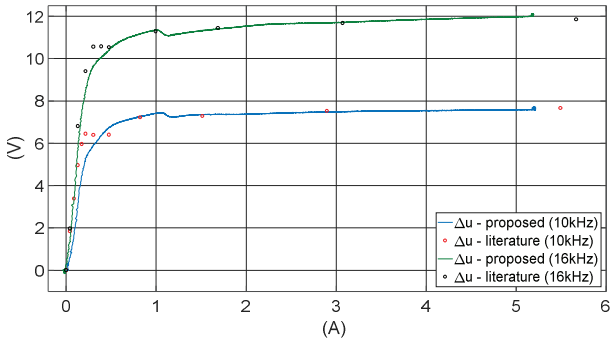

Fig. 12. Inverter phase voltage error as a function of current at 10 kHz and 16 kHz switching frequencies – comparison of the proposed method with that presented in [12].

with the dead-time unchanged (i.e. 2.5 µs). The dead-time effect with 16 kHz switching frequency causes a higher voltage error compared to 10 kHz case as seen in Fig. 12. The results in Fig. 12 are compared with the known method from [12].

As observed in Fig. 12, the proposed method gives a fairly accurate inverter error voltage estimate and the advantage is that the error characteristic can be obtained at a high resolution. The error characteristic is almost continuous and the resolution can be decided by the user by tapping voltage and current values at any interval of choice.

The gain $g_{\alpha\beta}$ in Fig. 4 plays an important role in allowing to get accurate error voltage characteristic. Effectively, it decides the bandwidth with which the error in (7) is corrected. If the error is corrected at a faster rate than the current ramp of

Fig. 11, the voltage $\Delta u_{\alpha\beta}$ will correspond to the actual current value. If the current ramp is too fast and the gain $g_{\alpha\beta}$ is not sufficient to eliminate the error, the voltage $\Delta u_{\alpha\beta}$ will not follow the actual inverter error in real time and the characteristic of Fig. 12 may not be reliable. In the results of Fig. 11, the current ramp has a slope of 1 A/s and the gain g is set equal to 100 rad/s for both α and β axes.

The advantages of using $g_{\alpha\beta}$ in Fig. 4 with respect to a past work [13] (where this gain is not present) are that (i) the time required for self-commissioning is independent of current steps (since the resolution is very fine here), (ii) the algorithm is independent of the bandwidth of current PI controllers, (iii) it is not necessary to wait for the steady state to be reached for recording the current and voltage values.

The disadvantage of the method proposed here (Fig. 4) is the dependence on the accuracy of machine parameters, namely, the stator resistance, the *d*- and *q*-axis inductances, and the PM flux-linkage. However, the dependence on parameters is not unique to the presented method, the works found in the literature also show parameter dependence to some extent. The effect of parameter errors is not analyzed in this paper but can be done in a future work.

Table II summarizes the results of parameter identification routines proposed in this paper. A comparison with known parameters is given and the percentage error in the estimation of each parameter is included.

TABLE II. ERRORS IN IDENTIFIED PARAMETERS

Quantity (unit)	*Known*	*Estimated*	*Error (%)*
Stator resistance (Ω)[2]	2.4	2.45	+2.1
d-axis inductance (mH)[1]	7.3	7.4	+1.4
q-axis inductance (mH)[1]	7.9	8.0	+1.3
PM flux-linkage (Vs)[2]	0.111	0.116	+4.5
Inverter error characteristic	Fig. 12	Fig. 12	--

[1] = PMLSM 1, [2] = PMLSM 2

VI. CONCLUSIONS

The paper discussed the identification of PMLSM machine parameters for drive controllers tuning. The presented methods use injected signals in a controlled manner to get parameter estimates in safest possible way. The self-commissioning procedure included the identification of inverter non-linearity characteristics. The identification tests were performed at standstill except for the estimation of PM flux-linkages for which carriage movement was inevitable. Compared to past work, the paper's major contributions were: (i) parameter identification of linear PM machines, (ii) presenting complete self-commissioning of the drive (motor + inverter), (iii) excluding the need for data post-processing, (iv) the high resolution of inverter non-linearity characteristic, and (v) no dependence on current PI controller bandwidth for inverter error identification. The obtained results showed that the parameters estimates were close to known values. The obtained inverter error voltage characteristic was compared with a known method from the literature and a good correlation was found.

REFERENCES

[1] J. F. Gieras, Z. J. Piech, and B. Z. Tomczuk, *Linear Synchronous Motors*, 2nd ed., CRC Press, Taylor & Francis Group, UK, 2011.

[2] S. Yang, K. Lin, "Automatic Control Loop Tuning for Permanent-Magnet AC Servo Motor Drives," *IEEE Trans. Ind. Electron.*, vol. 63, no. 3, pp. 1499-1506, Mar. 2016.

[3] Y.-S. Lai and M.-H. Ho, "Self-Commissioning Technique for High Bandwidth Servo Motor Drives," in *IEEE Energy Conversion Congress and Exposition (ECCE)*, 2017, pp. 342–349.

[4] L. Peretti, P. Sandulescu, and G. Zanuso, "Self-commissioning of flux linkage curves of synchronous reluctance machines in quasi-standstill condition," *IET Elect. Power Appl.*, vol. 9, no. 9, pp. 642-651, 2015.

[5] N. Bedetti, S. Calligaro, and R. Petrella, "Stand-Still Self-Identification of Flux Characteristics for Synchronous Reluctance Machines Using Novel Saturation Approximating Function and Multiple Linear Regression," *IEEE Trans. Ind. Appl.*, vol. 52, no. 4, pp. 3083-3092, Jul./Aug. 2016.

[6] S. Odhano, P. Giangrande, R. Bojoi, and C. Gerada, "Self-Commissioning of Interior Permanent-Magnet Synchronous Motor Drives With High-Frequency Current Injection," *IEEE Trans. Ind. Appl.*, vol. 50, no. 5, pp. 3295-3303, Sep./Oct. 2014.

[7] S. A. Odhano, R. Bojoi, S. G. Rosu, and A. Tenconi, "Identification of the Magnetic Model of Permanent-Magnet Synchronous Machines Using DC-Biased Low-Frequency AC Signal Injection," *IEEE Trans. Ind. Appl.*, vol. 51, no. 4, pp. 3208-3215, Jul./Aug. 2015.

[8] G. Pellegrino, "Identification of PM Synchronous Machines Parameters for Design and Control Purposes," book chapter from *The Rediscovery of Synchronous Reluctance and Ferrite Permanent Magnet Motors*, Springer International Publishing, 2016.

[9] S. Odhano, R. Bojoi, M. Popescu, and A. Tenconi, "Parameter Identification and Self-Commissioning of AC Permanent Magnet Synchronous Machines – A Review," in Proc. IEEE WEMDCD, Torino, Italy, Mar. 26-27, 2015, pp. 195-203.

[10] N. Bedetti, S. Calligaro, and R. Petrella, "Self-Commissioning of Inverter Dead-Time Compensation by Multiple Linear Regression Based on a Physical Model," *IEEE Trans. on Ind. Appl.*, vol. 51, no. 5, Sep./Oct.2015.

[11] A. Cichowski and J. Nieznanski, "Self-tuning dead-time compensation method for voltage-source inverters," *IEEE Power Electron. Lett.*, vol. 3, no. 2, pp. 72–75, Jun. 2005.

[12] R. Bojoi, E. Armando, G. Pellegrino, and S.G. Rosu, "Self-commissioning of inverter nonlinear effects in AC drives", Conf. Rec. IEEE ENERGYCON, 2012, pp. 213-218.

[13] G. Pellegrino, R. Bojoi, P. Guglielmi, and F. Cupertino, "Accurate Inverter Error Compensation and Related Self-Commissioning Scheme in Sensorless Induction Motor Drives," *IEEE Trans. Ind. Appl.*, vol. 46, no. 5, Sep./Oct. 2010.

[14] G. Pellegrino, P. Guglielmi, E. Armando, and R. I. Bojoi, "Self-Commissioning Algorithm for Inverter Nonlinearity Compensation in Sensorless Induction Motor Drives," *IEEE Trans. Ind. Appl.*, vol. 46, no. 4, pp. 1416–1424, Jul. 2010.

[15] J. Holtz and J. Quan, "Sensorless Vector Control of Induction Motors at Very Low Speed Using a Nonlinear Inverter Model and Parameter Identification," *IEEE Trans. Ind. Appl*, vol 38, no. 4, Jul./Aug. 2002.

[16] M. Ciobotaru, R. Teodorescu, and F. Blaabjerg, "A New Single-Phase PLL Structure Based on Second Order Generalized Integrator," in *37th IEEE Power Electronics Specialists Conference, PESC 2006*, pp. 1–6.

[17] V. Blahnik, T. Kosan, Z. Peroutka, and J. Talla, "Control of a Single-Phase Cascaded H-Bridge Active Rectifier Under Unbalanced Load," *IEEE Trans. Power Electron.*, vol. 33, no. 6, pp. 5519–5527, Jun. 2018.

[18] A. Bunte and H. Grotstollen, "Parameter identification of an inverter-fed induction motor at standstill with a correlation method," in *Fifth European Conference on Power Electronics and Applications*, 1993, vol. 5, pp. 97–102.

[19] R. Bojoi, E. Armando, F. Mariut, and S. Odhano, "Assessment method of dead-time compensation schemes of three-phase inverters using a hardware-in-the-loop configuration," in *2015 IEEE Energy Conversion Congress and Exposition, ECCE 2015*, pp. 4097–4104.

[20] A. Galassini, G. Lo Calzo, A. Formentini, C. Gerada, P. Zanchetta and A. Costabeber, "uCube: Control platform for power electronics," in Proc. IEEE WEMDCD, Nottingham, 2017, pp. 216-221.